PHYSICAL REVIEW B **90**, 085407 (2014)

Graphene band structure and its *2D* Raman mode

Rohit Narula* and Stephanie Reich
Fachbereich Physik, Freie Universität Berlin, Arnimallee 14, Berlin 14195, Germany
(Received 5 May 2014; revised manuscript received 16 July 2014; published 7 August 2014)

High-precision simulations are used to generate the *2D* Raman mode of graphene under a range of screening conditions and laser energies E_L. We reproduce the decreasing trend of the *2D* mode FWHM vs E_L and the nearly linearly increasing dispersion $\partial\omega_{2D}/\partial E_L$ seen experimentally in freestanding (unscreened) graphene, and propose relations between these experimentally accessible quantities and the local, two-dimensional gradients $|\nabla|$ of the electronic and *TO* phonon bands. In light of state-of-the-art electronic structure calculations that acutely treat the long-range *e-e* interactions of isolated graphene and its experimentally observed *2D* Raman mode, our calculations determine a 40% greater slope of the *TO* phonons about $\boldsymbol{K}$ than given by explicit phonon measurements performed in graphite or *GW* phonon calculations in graphene. We also deduce the variation of the broadening energy $\gamma[E_L]$ for freestanding graphene and find a nominal value $\gamma \sim 140$ meV, showing a gradually increasing trend for the range of frequencies available experimentally.

DOI: 10.1103/PhysRevB.90.085407 PACS number(s): 81.05.ue, 63.22.Rc, 78.67.Wj

I. INTRODUCTION

The *2D* Raman mode [1–3] is perhaps one of the most facile and widely accessed spectral features of graphene [4,5] and other sp^2 carbons such as nanoribbons and nanotubes [6]. The peculiar band structure of graphene [7], particularly around the $\boldsymbol{K}$ points of its Brillouin zone (BZ), endow it with a prominence [2,8,9] that is somewhat paradoxical given that it stems from a higher order (fourth order) of perturbation theory than the usual Γ point scattering (third order) as instantiated by the *G* mode. Also unlike the *G* mode, the *2D* mode has access to arbitrary phonon wave vectors $\boldsymbol{q}$ around $\boldsymbol{K}$ via a suitable choice of optical polarization and laser energy E_L [10,11]. The marriage of experimental and theoretical work has thus far established its ability to precisely determine phonon anharmonicities [12], doping [13], the number of graphene layers [14], phonon dispersion mapping [10,15], and the measurement of strain and crystalline orientation [11,16,17] in graphene, to name but a few.

Experimentally, the *2D* peak is often adequately described by a single Lorentzian [14]. However, recent measurements [18–20] of the broadened *2D* mode of suspended graphene have shown that a single Lorentzian profile becomes untenable at laser energies particularly in the infrared. The individual components of the observed bimodal shape have often been attributed to the so-called "inner" [21,22] and "outer" [14,15] processes [18,19]. By definition, the inner (outer) process corresponds to the dominant electronic transitions connecting the nearest (farthest) edges of equienergy contours corresponding to the laser energy E_L about the $\boldsymbol{K}$ and $\boldsymbol{K'}$ points with the $\boldsymbol{M}$ point lying halfway between them (see Fig. 1 of Ref. [10] for a schematic). They appear on account of an idealized one-dimensional description of the bands of graphene along its high-symmetry line: $\boldsymbol{\Gamma}$-$\boldsymbol{K}$-$\boldsymbol{M}$. However, we have already shown that the bifurcation into such processes is spurious [11]; the putative processes are indeed equivalent—modulo a reciprocal lattice vector. The question then arises, what is the origin of such an apparently bimodal peak? Even more puzzlingly, the full width at half maxima (FWHM) of the *2D* mode shows a decline with increasing excitation energy E_L. The predicted trend according to Ref. [18] is one of a sublinear increase of the FWHM vs E_L considering the estimated ratio v_{TO}/v_F and the dependence of the energy broadening $\gamma[E_L]$ of Ref. [23] in the expression $\text{FWHM} = 4\sqrt{2^{2/3}-1}\gamma v_{TO}/v_F$ of Basko [2] obtained from a simplified analytical model (see Fig. 5(b) of Ref. [18]).

The measurements of the *2D* mode of intrinsic, unsupported graphene (with very low doping) [18–20] are also interesting for they correspond to the limit of *unscreened* graphene, i.e., graphene unhindered by the additional screening contributed by the substrate. However most of the experimental *2D* Raman spectra have been obtained from supported or sandwiched graphene, which is therefore at least *partially screened*. Since both the electronic bands of graphene [24] and its *TO* phonon band—with its peculiar Kohn anomaly [25,26]—are strongly affected by screening, it would be illuminating to rationalize the features of the *2D* mode as a function of electronic screening effects.

In this article we present the results of high-precision transition matrix $\mathcal{T}_{fi}[\boldsymbol{q}]$ simulations of graphene's *2D* Raman spectra combining perturbation theory with *ab initio* electronic and phonon band structure and matrix element calculations. Our simulations fully address the two-dimensional BZ of graphene and the characteristic trigonal warping [7] of both the electronic and *TO* phonon bands that is indispensable at the laser energies employed in practice [11] [see the isoenergy contours of Figs. 4(a)–4(c), and the *TO* phonon contours of Fig. 5(a)]. We consider four pairings of the electronic and phonon bands reflecting different levels of screening, including one that considers the idealized but instructive case of a flat, nondispersive *TO* band. We achieve a favorable correspondence with the decreasing *2D* FWHM vs E_L and nearly linearly increasing dispersion as observed in Ref. [18]. Inspired by idealized analytical models and fine-tuned by a multitude of simulations we propose simple yet robust relations among the dispersion and FWHM of the *2D* mode as a function of the ratio of *local* absolute gradient of

*narula@physik.fu-berlin.de

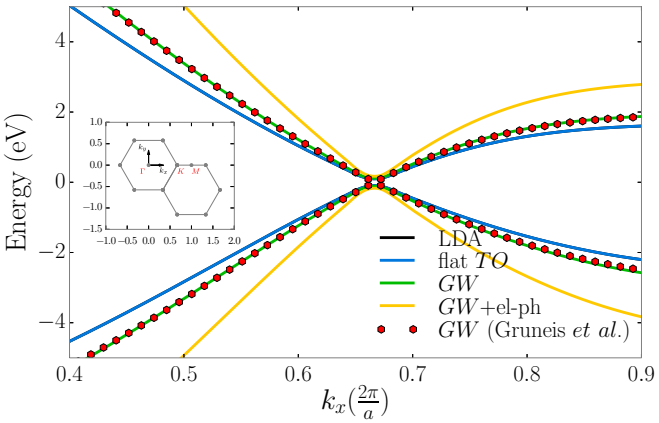

FIG. 1. (Color online) The valence and conduction bands of undoped graphene (Fermi energy: $E_F = 0.0$ eV) generated according to Eq. (1) and the values of the parameters e_f listed in Table. I. They correspond to an increasing degree of sophistication of *ab initio* techniques (LDA $\rightarrow$ GW $\rightarrow$ GW + el-ph), or, alternatively, decreasing amounts of screening prevalent in the graphene monolayer. The red circles represent the tight-binding fit to GW electronic band calculations of Ref. [28].

the $2 \times TO$ phonon band $|\nabla\omega_{2TO}[E_L]|$ and the gradient of the difference between the conduction and valence bands $|\nabla E_g[E_L]| = |\nabla(E_c[E_L] - E_v[E_L])|$.

II. CALCULATION DETAILS

The *2D* Raman mode was modeled via the transition matrix $\mathcal{T}_{fi}[\boldsymbol{q}]$ [11] (the mode intensity $I_{2D} \propto |\mathcal{T}_{fi}[\boldsymbol{q}]|^2$) that is described in detail in the Appendix. This perturbational approach is standard and has been successfully used to study the *2D* mode [2,8,11,23,27]. The ingredient electronic valence and conduction ($E_v^{\rm LDA}[\boldsymbol{k}]$, $E_c^{\rm LDA}[\boldsymbol{k}]$) and phonon bands ($\omega_{TO}^{\rm LDA}[\boldsymbol{q}]$) and the associated optical and electron-phonon matrix elements were explicitly obtained over the entire two-dimensional BZ of graphene via *ab initio* calculations as described in Ref. [11]. The actual electronic dispersions used in our calculations, $E_v[\boldsymbol{k}]$, $E_c[\boldsymbol{k}]$ (see Fig. 1), were obtained by deforming the LDA-derived bands $E_c^{\rm LDA}[\boldsymbol{k}]$, $E_v^{\rm LDA}[\boldsymbol{k}]$ according to

$$E_v[\boldsymbol{k}] = e_f\big(E_v^{\rm LDA}[\boldsymbol{k}] - E_F\big) + E_F, \tag{1a}$$

$$E_c[\boldsymbol{k}] = e_f\big(E_c^{\rm LDA}[\boldsymbol{k}] - E_F\big) + E_F, \tag{1b}$$

where E_F is the Fermi energy, and the parameter e_f is as listed in Table I. The particular form of Eq. (1) was especially chosen to preserve all the attendant symmetries present in the two-dimensional LDA electronic bands. The case labeled "GW" follows the tight-binding fit to GW electronic band calculations of Grüneis *et al.* [28], representing the case of partial screening. "GW + el-ph" represents the calculations of Siegel *et al.* [24] corresponding to the limit of unscreened graphene. The LDA bands, $E_v^{\rm LDA}[\boldsymbol{k}]$, $E_c^{\rm LDA}[\boldsymbol{k}]$, on the other hand, represent the opposite limit of fully screened graphene.

The phonon bands $\omega_{TO}[\boldsymbol{q}]$ were obtained from $\omega_{TO}^{\rm LDA}[\boldsymbol{q}]$ via

$$\omega_{TO}[\boldsymbol{q}] = \omega_{TO}^{\rm LDA}[\boldsymbol{q}] - p_f\big(\omega_{TO}^{\rm LDA}[\boldsymbol{q}] - c\big) + p_o, \tag{2}$$

TABLE I. The parameters used to generate the electronic and *TO* phonon bands of Eqs. (1) and (2), respectively. v_F is the calculated average of the conduction and valence band slopes, each along the $\boldsymbol{K}$-$\boldsymbol{\Gamma}$ and $\boldsymbol{K}$-$\boldsymbol{M}$ directions. $\alpha_{\boldsymbol{K}}$ is the slope of the *TO* phonon dispersion about the $\boldsymbol{K}$ point.

	LDA (fully screened)	GW (partially screened)	GW+ el-ph (unscreened)	flat *TO*	
electrons					
e_f	1.00	1.17	1.74	1.00	
v_F	0.85	1.01	1.48	0.85	10^6 $\frac{\rm m}{\rm s}$
TO phonon					
p_f	0.00	−0.80	−1.50	1.00	
p_o	0	−75	−35	0	$\rm cm^{-1}$
c	1389	1389	1389	1389	$\rm cm^{-1}$
$\alpha_{\boldsymbol{K}}$	901	1622	2253	0	$\rm cm^{-1}$

that likewise preserves all the peculiar symmetries inherent in the LDA-derived *TO* phonons. The values of the parameters p_f, p_o, and c are listed in Table I. The *TO* phonon bands labeled "GW" were obtained by fitting the GW calculations of Lazzeri *et al.* [25] (green diamonds of Fig. 2), and are also a good match for the inelastic x-ray scattering (IXS) experiments in graphite of Ref. [29] as shown by the red circles in Fig. 2. The phonon bands entitled "GW + el-ph" (see yellow curve of Fig. 2) were determined *a posteriori* from the combination of experimental data of Ref. [18] and our simulations. The computation of $\mathcal{T}_{fi}[\boldsymbol{q}]$ required resampling the fully two-dimensional bands and matrix elements on a grid with a density exceeding 5700 $\times$ 5700 per BZ [30] for both $\boldsymbol{k}$ and $\boldsymbol{q}$. The laser excitation energies E_L investigated were in the range 1.2–2.8 eV in steps of 0.2 eV. The stringent sampling was dictated by the requirements of

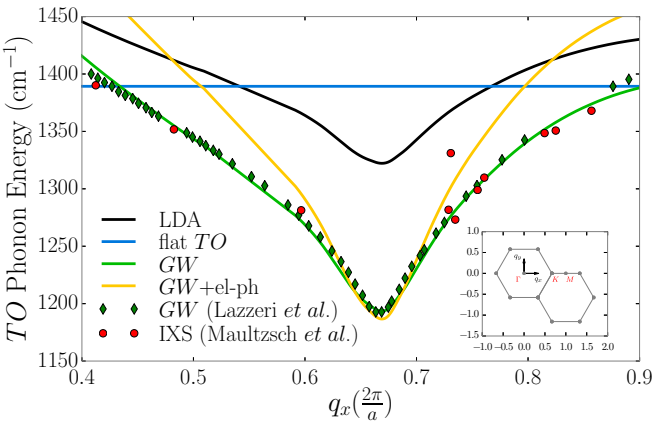

FIG. 2. (Color online) The *TO* phonon dispersions of graphene generated according to Eq. (2) and the values of the parameters p_f, p_o, and c listed in Table. I. They correspond to a progression of first-principles approaches (LDA $\rightarrow$ GW $\rightarrow$ GW + el-ph), or, alternatively, decreasing amounts of screening operating in the graphene monolayer. The green diamonds are the values of the GW phonon calculation of graphene's *TO* band from Ref. [25]. The red circles represent the IXS measurements of the *TO* band of graphite from Ref. [29].

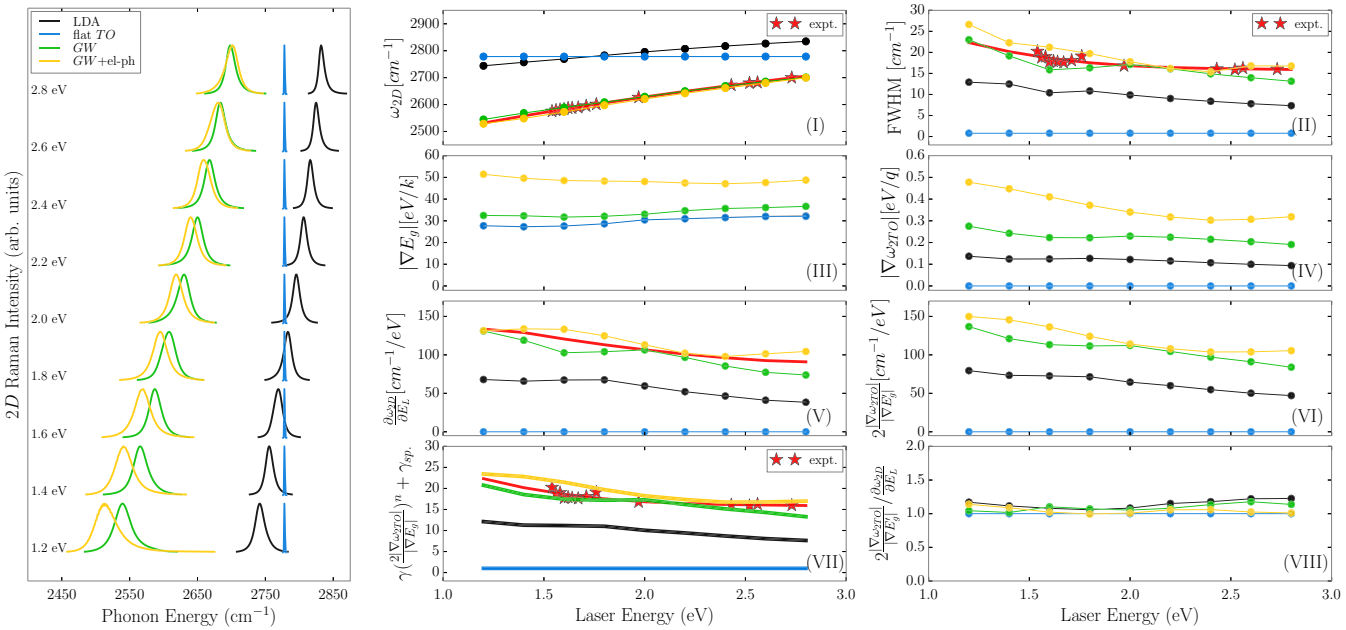

FIG. 3. (Color online) The leftmost panel shows the calculated *2D* Raman spectra for the electronic and *TO* phonon bands of Eqs. (1) and (2) and the values of the parameters given in Table I. Panel (I) shows the mean *2D* mode frequencies ω_{2D} as a function of laser energy E_L while (II) shows the *2D* mode FWHM vs E_L. The experimental *2D* Raman spectra of suspended graphene from Ref. [18] are represented by red stars and by third-order polynomial fits given by red lines. Panels (III) and (IV) show the variation of the absolute gradients $|\nabla E_g[E_L]|$ and $|\nabla\omega_{2TO}[E_L]|$ and can be compared with Figs. 4(a)–4(f), respectively. Panel (V) shows the calculated *2D* mode dispersion $\frac{\partial\omega_{2D}}{\partial E_L}$ while panel (VI) shows the quantity $2\frac{|\nabla\omega_{2TO}|}{|\nabla E_g|}$. Panel (VII) shows a model fit to the calculated FWHM according to Eq. (15) with $n \sim 0.98$ and $\gamma_{sp} = 1.0$ cm^{-1}. Finally, panel (VIII) shows the ratio of the model $2\frac{|\nabla\omega_{2TO}|}{|\nabla E_g|}$ of panel (VI) and calculated values $\frac{\partial\omega_{2D}}{\partial E_L}$ of panel (V), which is very close to 1.0, as desired.

capturing a realistic Raman spectrometer resolution of $\gamma_{sp} = 1$ cm^{-1} as modeled by convolving $\mathcal{T}_{fi}[\boldsymbol{q}]$ with Gaussians of the same FWHM. The broadening energies γ were assumed identical for all the transitions in $\mathcal{T}_{fi}[\boldsymbol{q}]$. γ was taken constant as a function of E_L primarily for clarity of exposition, but does not affect the veracity of the fitting expression proposed in Eq. (15). The value $\gamma = 130$ meV was selected for providing a nominal correspondence for cases GW and GW + el-ph with the experimentally observed *2D* FWHM vs E_L and dispersion of Ref. [18].

III. RESULTS AND DISCUSSION

The leftmost panel of Fig. 3 shows the calculated *2D* Raman spectra. The averaged mode frequencies ω_{2D} [31] for the case GW + el-ph are in accord with the experimental findings [red stars in Fig. 3, panel (I)] in freestanding graphene of Ref. [18]. The case GW has a similar dispersion but occurs at marginally higher phonon frequencies, corresponding closely with the *2D* mode measurements on supported graphene in Ref. [18]. The LDA case reflects a profile that is much flatter and higher in frequency than the GW and GW + el-ph scenarios owing to the weaker Kohn anomaly around $\boldsymbol{K}$ for the LDA case [25]. The nondispersive phonons for flat *TO* expectedly show a stationary *2D* mode profile. Apart from flat *TO*, the spectra stemming from the dispersive *TO* phonons of cases LDA, GW, and GW + el-ph (see Fig. 2) evidence a decreasing FWHM [32] with E_L [see Fig. 3, panel (II)] in good agreement with Ref. [18] [red stars in Fig. 3, panel (II)].

For the nondispersive flat *TO* case, the FWHM is simply equal to the spectrometer resolution $\gamma_{sp} = 1$ cm^{-1}:

$$\nabla = \frac{\partial}{\partial x}\hat{i} + \frac{\partial}{\partial y}\hat{j}, \tag{3a}$$

$$|\nabla a[x,y]| = \sqrt{\frac{\partial a[x,y]}{\partial x}^2 + \frac{\partial a[x,y]}{\partial y}^2}. \tag{3b}$$

We followed the absolute gradient $|\nabla|$ as defined in Eqs. (3a) and (3b) of the difference between the conduction and valence bands $E_g[\boldsymbol{k}] = E_c[\boldsymbol{k}] - E_v[\boldsymbol{k}]$ [see Fig. 3, panel (III)] and the $2 \times TO$ phonon band. While $|\nabla E_g|$ remains relatively flat as a function of E_L, $|\nabla\omega_{2TO}|$ [see Fig. 3, panel (IV)] decreases sharply in the range 1.2–2.0 eV but then flattens out at higher laser energies. Seen over the entire electronic reciprocal space, $|\nabla E_g[\boldsymbol{k}]|$ [see Figs. 4(a)–4(c)] increases going from the cases LDA, GW, and GW + el-ph, reflecting their increasing v_F as listed in Table I. Similarly, $|\nabla\omega_{2TO}[\boldsymbol{q}]|$ [see Figs. 4(d)–4(f)] increases as the Kohn anomaly gets more prominent as the level of screening is reduced, culminating in the case GW + el-ph.

The calculated dispersion of the averaged *2D* mode frequency $\partial\omega_{2D}/\partial E_L$ [see Fig. 3, panel (V)] is found to be excellently captured by the expression $2\frac{|\nabla\omega_{2TO}|}{|\nabla E_g|}$ [see Fig. 3, panel (VI)] over the entire range of excitation energies E_L and across all the combinations of electrons and *TO* phonons considered. The goodness of fit is captured by the ratio $2\frac{|\nabla\omega_{2TO}|}{|\nabla E_g|}/\frac{\partial\omega_{2D}}{\partial E_L}$ [see Fig. 3, panel (VIII)] that is remarkably stable

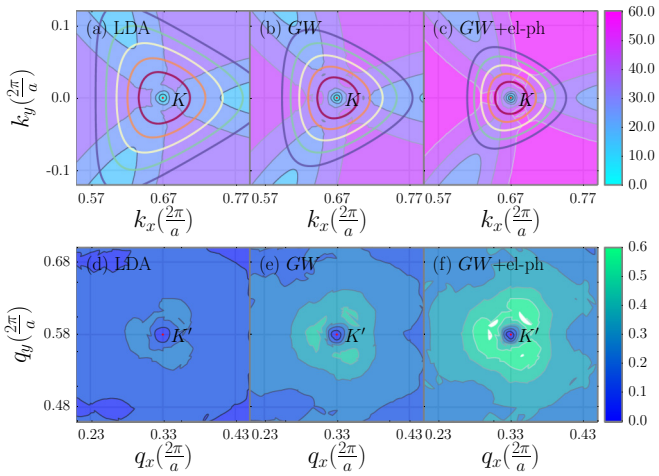

FIG. 4. (Color online) (a)–(c) depict the absolute gradients $|\nabla E_g[\boldsymbol{k}]| = |\nabla(E_c[\boldsymbol{k}] - E_v[\boldsymbol{k}])|$ over the two-dimensional electronic reciprocal space $\boldsymbol{k}$. The trigonal contours represent excitation energies E_L from 1.0 to 3.0 eV (incl.) in steps of 0.5 eV. Compare with Fig. 3, panel (III). Panels (d)–(e) show the absolute gradients $|\nabla\omega_{2TO}[\boldsymbol{q}]|$ over the phonon reciprocal space $\boldsymbol{q}$. Compare with Fig. 3, panel (IV). Both the electronic $|\nabla E_g[\boldsymbol{k}]|$ and *TO* phonon gradients $|\nabla\omega_{2TO}[\boldsymbol{q}]|$ show a secular increase as the screening is lowered.

with an average value of 1.1 across the range of E_L considered. We thus propose the relation

$$\frac{\partial\omega_{2D}}{\partial E_L}[E_L]_{\text{fit}} = 1.1 \times 2\frac{|\nabla\omega_{2TO}[E_L]|}{|\nabla E_g[E_L]|}. \tag{4}$$

This result can be rationalized by considering conical electronic and *TO* phonon bands around the $\boldsymbol{K}$ points. For the *TO* phonon dispersion we have

$$\omega_{TO} = \omega^0_{TO} + v_{\text{ph}}\sqrt{\boldsymbol{q}^2_{x,\boldsymbol{K}'} + \boldsymbol{q}^2_{y,\boldsymbol{K}'}}, \tag{5}$$

which becomes for the ω_{2D} phonon dispersion

$$\omega_{2D} = 2\omega^0_{TO} + 2\,v_{\text{ph}}\sqrt{\boldsymbol{q}^{*2}_{x,\boldsymbol{K}'} + \boldsymbol{q}^{*2}_{y,\boldsymbol{K}'}}. \tag{6}$$

Similarly, we can write for the difference E_g between the conduction and valence bands,

$$E_g = (v_c - v_v)\sqrt{\boldsymbol{k}^2_{x,\boldsymbol{K}} + \boldsymbol{k}^2_{y,\boldsymbol{K}}}, \tag{7}$$

which at resonance ($E_g = E_L$) takes the form

$$E_L = (v_c - v_v)\sqrt{\boldsymbol{k}^{*2}_{x,\boldsymbol{K}} + \boldsymbol{k}^{*2}_{y,\boldsymbol{K}}}. \tag{8}$$

Adapting the relationship derived in Ref. [1] for the dominant phonon wave vectors $\boldsymbol{q}^*$ of the *2D* mode we get

$$\boldsymbol{q}^*_{\boldsymbol{K}'} = 2\left(\frac{E_L - \omega_{TO}}{v_c - v_v}\right) \tag{9}$$

$$\approx 2\left(\frac{E_L}{v_c - v_v}\right) \tag{10}$$

$$\approx 2\boldsymbol{k}^*_{\boldsymbol{K}}, \tag{11}$$

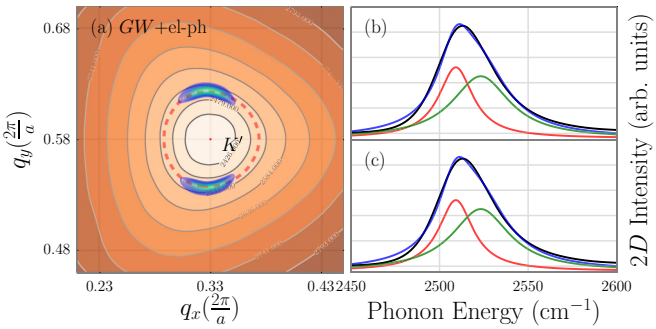

FIG. 5. (Color online) (a) The orange-hued phonon energy contours of $2 \times TO$ band about $\boldsymbol{K}$ for the GW + el-ph case superimposed with dominant phonon wave vectors $\boldsymbol{q}^*$ (green-blue) of the *2D* Raman mode for $E_L = 1.2$ eV. The polarizer and analyzer are set along the zigzag orientation of graphene. The dotted red lines correspond to $\boldsymbol{q}^*$ of Eq. (16). The contributions of the phonon wave vectors above and below the $\boldsymbol{K}$ point give rise to identical spectra as shown in panels (b) and (c).

where v_v and v_c are the Fermi velocities of the conduction and valence bands, respectively, and where for simplicity we have neglected the phonon energy ω_{2TO} as $E_L \gg \omega_{2TO}$.

Using the definitions of Eqs. (3a), (3b), and (6) we find that

$$|\nabla\omega_{2D}| = |\nabla\omega_{2TO}| = 2v_{\text{ph}}, \tag{12}$$

while using Eqs. (3a), (3b), and (7) we obtain

$$|\nabla E_g| = v_c - v_v. \tag{13}$$

Using Eq. (11) and Eqs. (6) and (7) and the above relations we finally obtain

$$\frac{\partial\omega_{2D}}{\partial E_L} = 2\frac{|\nabla\omega_{2TO}|}{|\nabla E_g|}, \tag{14}$$

which is nearly identical to Eq. (4), as desired.

We found that the FWHMs shown in Fig. 3, panel (II), are well fitted by the expression given in Eq. (15),

$$\text{FWHM}[E_L]_{\text{fit}} = \gamma[E_L]\left(2\frac{|\nabla\omega_{2TO}[E_L]|}{|\nabla E_g[E_L]|}\right)^{0.98} + \gamma_{sp}, \tag{15}$$

which is reminiscent of the analytical expression derived by Basko [2]: $\text{FWHM} = 4\sqrt{2^{2/3}-1}\gamma v_{TO}/v_F$. Figure 5(a) shows $\boldsymbol{q}^*$ for the *2D* mode corresponding to the GW + el-ph case superimposed on the $2 \times TO$ phonon dispersion for the polarizer and analyzer both parallel to the zigzag orientation of graphene. Our calculations and a combination of Eqs. (11)–(13) confirm that $\boldsymbol{q}^*$ [see Fig. 5(a)] is related to $\boldsymbol{k}^*$ [see Figs. 4(a)–4(c)] as

$$\boldsymbol{q}^* = \frac{2(\boldsymbol{k}^* - \boldsymbol{K})}{1 + \frac{|\nabla\omega_{2TO}|}{|\nabla E_g|}} + \boldsymbol{K}', \tag{16}$$

while the precise location of the two (spectrally equivalent) regions of $\boldsymbol{q}^*$ around $\boldsymbol{K}'$ is determined by the polarizer:analyzer combination as explained in Refs. [10,11]. Our calculations show that the $\boldsymbol{q}^*$ above and below the $\boldsymbol{K}'$ point contribute to identical *2D* spectra [33]. The resultant spectra can only be fitted adequately by a sum of at least two Lorentzians as is shown by the red and green Lorentzian subspectra in Figs. 5(b)

or 5(c). Looking at the green-blue shaded region for $\boldsymbol{q}^*$ of Fig. 5(a) we find that each is contiguous, with no discernible substructure and for a large part traverses a region that falls outside the high-symmetry lines [11]. Thus, we conclude that both the component Lorentzians in the observed spectra stem from the same (or equivalent) region of $\boldsymbol{q}^*$ space. Naturally, both the component Lorentzians, that are often labeled as $2D^-$ and $2D^+$ [18] and (mistakenly) attributed to the inner and outer processes, have therefore nearly the same slope as observed experimentally [18]. Consequently, there appears to be no reason to distinguish between the origins of the individual Lorentzians used to fit the observed *2D* spectra. Basically, the *2D* line shape is intrinsically non-Lorentzian as demonstrated by the experimental spectra and our calculations. Whereas a non-Lorentzian line shape was also evident in the simplified analytical work of Ref. [2], intuitively the nonsymmetric nature of the *2D* peak also stands to reason given that the *2D* spectra involves an interplay between the electronic and the *TO* phonon bands that are both highly dispersive. This intuition may be made more concrete by considering that $|\nabla\omega_{2TO}| \ll |\nabla E_g|$ [see Fig. 3, panels (III) and (IV)] and therefore $\boldsymbol{q}^*$ of Eq. (16) [see green-blue regions of Fig. 5(a), for instance] depends almost wholly on the details of the electronic dispersion. Only for the nondispersive *TO* phonons (flat *TO*) do we recover a symmetric peak [34]. When the phonons are highly dispersive, as expected in cases where the electronic screening is minimized such as for suspended graphene (GW + el-ph), we should expect a broadened *2D* peak refractory to fitting by a single Lorentzian.

Unlike an ordinary metal, graphene is anticipated to show a departure from normal Fermi level liquid behavior particularly near the Dirac point owing to its semimetallic character [24]. This departure is especially severe in the low screening limit of freestanding graphene, as opposed to supported graphene where the substrate contributes additional screening. First-principles calculations [24] properly taking into account the long-range *e-e* interactions to the self-energy show that $v_F = 1.48 \times 10^6$ m/s for freestanding graphene is substantially higher than the usual value of $v_F \sim 1.10 \times 10^6$ m/s from scanning tunneling microscopy experiments on supported graphene (graphene on SiC) [35] and GW calculations [28]. Combining the increased v_F for the case of freestanding graphene with the experimental *2D* mode observations of Ref. [18] in our calculations gives an *a posteriori* slope $\alpha_{\boldsymbol{K}}$ [36] of the *TO* phonon dispersion that is 40% steeper (see yellow curve of Fig. 2) about $\boldsymbol{K}$ than given by the GW phonon calculations in graphene (see green curve of Fig. 2) of Ref. [25] which hitherto were considered state-of-the-art. The higher v_F and the steeper α_K of the GW-el-ph case also strongly affects the square of the electron-phonon coupling (EPC) $\langle g^2_{\boldsymbol{K}}\rangle_F \propto \alpha_K v_F$ [37], becoming twice as high as the GW value and therefore likely to strongly affect the high-bias current transport [38] and phonon lifetimes [12] of freestanding graphene. For the range of available experimental data [18], γ is found to increase gently with E_L (see Fig. 6) as deduced from Eqs. (4) and (15). Although this general trend is consistent with the model proposed by Venezuela *et al.* [23] (green curve of Fig. 6), the values from our calculations are significantly higher (roughly, a factor of 2) and with a much lower dispersion. Several possible sources for this discord can be identified. One

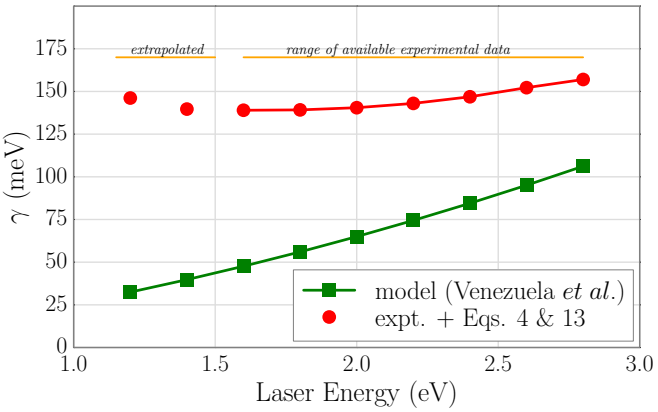

FIG. 6. (Color online) The energy broadening γ vs laser energy E_L (in red) deduced from the *2D* mode experimental spectra of suspended graphene of Ref. [18] and Eqs. (4) and (15). Due to the paucity of experimental data [18] the region to be relied upon lies within ~1.6 to 2.8 eV, whereas the region delineated from 1.0 to 1.5 eV is extrapolated. The model in green is taken from Ref. [23].

is that the calculations performed in Ref. [23] are performed within the GW approximation for the electron and phonon energies, while the eigenfunctions and therefore the matrix elements are left unperturbed from the basal LDA calculation. Indeed, we have determined that the square of the EPC $\langle g^2_{\boldsymbol{K}}\rangle_F$ is twice as high as from GW calculations. Second, as pointed out by Ref. [24], in the limit of freestanding graphene where the electronic screening is minimized, the *e-e* interactions strongly renormalize the electronic band structure around the Dirac point (see the electronic bands for the case GW + el-ph in Fig. 1), thus requiring a theoretical machinery going beyond the GW approximation. Similar considerations apply for the *TO* phonon band wherein we anticipate the Kohn anomaly [26] to be more severe for freestanding graphene. This hypothesis is consistent with the 40% steeper *TO* dispersion for the case GW + el-ph, which explains the observed *2D* spectra of Ref. [18] and the electronic structure calculations of Ref. [24] with a high degree of correspondence. In this context, it is important to consider that nearly all the explicit experimental measurements of the *TO* phonons, typically used as an *ersatz* for graphene, have been performed instead for graphite [29,39]. Other possibilities include neglecting the explicit dependence of γ on $\boldsymbol{k}$ [40] and the approximation of using an identical γ across all transitions in our calculation of $\mathcal{T}_{fi}[\boldsymbol{q}]$.

IV. SUMMARY AND OUTLOOK

In summary, our simulations have reproduced the characteristic features of the experimental *2D* Raman mode in freestanding graphene including the line shape, the decreasing FWHM vs E_L, and the dispersion. Our results for the GW + el-ph or unscreened case when combined with the band structure dispersion, as given by the state-of-the-art electronic structure calculations of Siegel *et al.* [24], determine that the *TO* phonon band has a 40% steeper dispersion about $\boldsymbol{K}$ than given by explicit phonon measurements in graphite [29,39] and the GW calculations of Ref. [25]. We were able to demonstrate robust

relationships among the *2D* mode dispersion $\partial\omega_{2D}/\partial E_L$, and FWHM as a function of the local gradients $|\nabla|$ of the electronic bands and *TO* phonon bands as given in Eqs. (4) and (15). These relations provide the experimentalist with an accurate method to relate the routinely measured information regarding the *2D* mode with the details of the two-dimensional electronic bands and the *TO* phonon dispersion. We deduced the energy broadening γ as a function of E_L for the experimental data from freestanding graphene of Ref. [18] and found a gentle increase with E_L with a nominal value of $\gamma \sim 140$ meV.

The nominally bimodal, nonsymmetric *2D* mode line shape, resistant to fitting with a single Lorentzian, especially for freestanding graphene and/or infrared laser excitation, arises primarily because of the dispersiveness of both the electronic and *TO* phonon bands. Indeed, for the case of nondispersive *TO* phonons (flat *TO*) we found that the peak is perfectly symmetric and reflects merely the spectral response of the Raman spectrometer modeled to be symmetric in this work. The location of $\boldsymbol{q}^*$ are determined almost completely by the details of the electronic dispersion, while the spectral range or width of the *2D* Raman peak is proportional to $|\nabla_{2TO}[\boldsymbol{q}^*]|$.

As the *2D* mode dispersion depends on the ratio $2\frac{|\nabla\omega_{2TO}[E_L]|}{|\nabla E_g[E_L]|}$, it is difficult to infer the level of screening from the observed Raman spectra since two wholly different combinations of electron and *TO* phonon bands may yield a similar dispersion [compare the cases *GW* and *GW* + el-ph in Fig. 3, panel (I)]. This points to the need for further research to elucidate the precise interrelationships among the electronic and phonon bands and the relevant broadening energies as a function of screening, which may then be used in conjunction with Raman spectroscopy [via Eqs. (4) and (15)] to make a finer assessment.

ACKNOWLEDGMENT

Parts of this work were supported by the European Research Council (ERC) under Grant No. 210642.

APPENDIX

The transition matrix $\mathcal{T}_{fi}[\boldsymbol{q}]$ [11] from fourth-order perturbation theory, within the free-particle picture reads

$$\mathcal{T}_{fi}[\boldsymbol{q}] = \sum_{\boldsymbol{k}} \frac{\langle v,\boldsymbol{k}-\boldsymbol{q}|H_{e-R}|c,\boldsymbol{k}-\boldsymbol{q}\rangle\langle v,\boldsymbol{k}-\boldsymbol{q}|H_{e-\mathrm{ph}}|v,\boldsymbol{k}\rangle^{\dagger}\langle c,\boldsymbol{k}-\boldsymbol{q}|H_{e-\mathrm{ph}}|c,\boldsymbol{k}\rangle\langle c,\boldsymbol{k}|H_{e-R}|v,\boldsymbol{k}\rangle}{\{E_L-(E_c[\boldsymbol{k}-\boldsymbol{q}]-E_v[\boldsymbol{k}-\boldsymbol{q}])-2\omega_{TO}[\boldsymbol{q}]+\imath\gamma[E_L]\}\{E_L-(E_c[\boldsymbol{k}-\boldsymbol{q}]-E_v[\boldsymbol{k}])-\omega_{TO}[\boldsymbol{q}]+\imath\gamma[E_L]\}\{E_L-(E_c[\boldsymbol{k}]-E_v[\boldsymbol{k}])+\imath\gamma[E_L]\}}$$
$$+\frac{\langle v,\boldsymbol{k}-\boldsymbol{q}|H_{e-R}|c,\boldsymbol{k}-\boldsymbol{q}\rangle\langle c,\boldsymbol{k}-\boldsymbol{q}|H_{e-\mathrm{ph}}|c,\boldsymbol{k}\rangle\langle v,\boldsymbol{k}-\boldsymbol{q}|H_{e-\mathrm{ph}}|v,\boldsymbol{k}\rangle^{\dagger}\langle c,\boldsymbol{k}|H_{e-R}|v,\boldsymbol{k}\rangle}{\{E_L-(E_c[\boldsymbol{k}-\boldsymbol{q}]-E_v[\boldsymbol{k}-\boldsymbol{q}])-2\omega_{TO}[\boldsymbol{q}]+\imath\gamma[E_L]\}\{E_L-(E_c[\boldsymbol{k}]-E_v[\boldsymbol{k}-\boldsymbol{q}])-\omega_{TO}[\boldsymbol{q}]+\imath\gamma[E_L]\}\{E_L-(E_c[\boldsymbol{k}]-E_v[\boldsymbol{k}])+\imath\gamma[E_L]\}}$$
$$+\frac{\langle v,\boldsymbol{k}|H_{e-R}|c,\boldsymbol{k}\rangle\langle c,\boldsymbol{k}|H_{e-\mathrm{ph}}|c,\boldsymbol{k}-\boldsymbol{q}\rangle\langle c,\boldsymbol{k}-\boldsymbol{q}|H_{e-\mathrm{ph}}|c,\boldsymbol{k}\rangle\langle c,\boldsymbol{k}|H_{e-R}|v,\boldsymbol{k}\rangle}{\{E_L-(E_c[\boldsymbol{k}]-E_v[\boldsymbol{k}])-2\omega_{TO}[\boldsymbol{q}]+\imath\gamma[E_L]\}\{E_L-(E_c[\boldsymbol{k}-\boldsymbol{q}]-E_v[\boldsymbol{k}])-\omega_{TO}[\boldsymbol{q}]+\imath\gamma[E_L]\}\{E_L-(E_c[\boldsymbol{k}]-E_v[\boldsymbol{k}])+\imath\gamma[E_L]\}}$$
$$+\frac{\langle c,\boldsymbol{k}|H_{e-R}|v,\boldsymbol{k}\rangle^{\dagger}\langle v,\boldsymbol{k}|H_{e-\mathrm{ph}}|v,\boldsymbol{k}-\boldsymbol{q}\rangle^{\dagger}\langle v,\boldsymbol{k}-\boldsymbol{q}|H_{e-\mathrm{ph}}|v,\boldsymbol{k}\rangle^{\dagger}\langle v,\boldsymbol{k}|H_{e-R}|c,\boldsymbol{k}\rangle^{\dagger}}{\{E_L-(E_c[\boldsymbol{k}]-E_v[\boldsymbol{k}])-2\omega_{TO}[\boldsymbol{q}]+\imath\gamma[E_L]\}\{E_L-(E_c[\boldsymbol{k}]-E_v[\boldsymbol{k}-\boldsymbol{q}])-\omega_{TO}[\boldsymbol{q}]+\imath\gamma[E_L]\}\{E_L-(E_c[\boldsymbol{k}]-E_v[\boldsymbol{k}])+\imath\gamma[E_L]\}},$$

where H_{e-R} is the Hamiltonian corresponding to the light-matter interaction and $H_{e-\mathrm{ph}}$ is the Hamiltonian representing electron-phonon coupling. The electronic eigenstates (e.g., $|c,\boldsymbol{k}\rangle$) are labeled by their branch index (c: conduction band, v: valence band) and wave vector k. The band energies, as a function of the electronic wave vector k, are denoted by $E_v[\boldsymbol{k}]$ and $E_c[\boldsymbol{k}]$ for the valence and conduction bands of graphene, respectively, while the *TO* phonon dispersion, as a function of the phonon wave vector $\boldsymbol{q}$, is $\omega_{TO}[\boldsymbol{q}]$. E_L is the incident laser energy and $\gamma[E_L]$ is the energy broadening term.

[1] C. Thomsen and S. Reich, Phys. Rev. Lett. **85**, 5214 (2000).
[2] D. M. Basko, Phys. Rev. B **78**, 125418 (2008).
[3] R. Narula, Ph.D. thesis, Massachusetts Institute of Technology, 2011.
[4] K. S. Novoselov, A. K. Geim, S. V. Morozov, D. Jiang, Y. Zhang, S. V. Dubonos, I. V. Grigorieva, and A. A. Firsov, Science **306**, 666 (2004).
[5] A. K. Geim and K. S. Novoselov, Nat. Mater. **6**, 183 (2007).
[6] S. Reich and C. Thomsen, Philos. Trans. R. Soc., A **362**, 2271 (2004).
[7] P. R. Wallace, Phys. Rev. **71**, 622 (1947).
[8] R. Narula and S. Reich, Phys. Rev. B **78**, 165422 (2008).
[9] R. Narula, R. Panknin, and S. Reich, Phys. Rev. B **82**, 045418 (2010).
[10] R. Narula, N. Bonini, N. Marzari, and S. Reich, Phys. Status Solidi B **248**, 2635 (2011).
[11] R. Narula, N. Bonini, N. Marzari, and S. Reich, Phys. Rev. B **85**, 115451 (2012).
[12] N. Bonini, M. Lazzeri, N. Marzari, and F. Mauri, Phys. Rev. Lett. **99**, 176802 (2007).
[13] S. Pisana, M. Lazzeri, C. Casiraghi, K. S. Novoselov, A. K. Geim, A. C. Ferrari, and F. Mauri, Nat. Mater. **6**, 198 (2007).
[14] A. C. Ferrari, J. C. Meyer, V. Scardaci, C. Casiraghi, M. Lazzeri, F. Mauri, S. Piscanec, D. Jiang, K. S. Novoselov, S. Roth, and A. K. Geim, Phys. Rev. Lett **97**, 187401 (2006).
[15] R. Saito, A. Jorio, A. G. Souza Filho, G. Dresselhaus, M. S. Dresselhaus, and M. A. Pimenta, Phys. Rev. Lett. **88**, 027401 (2001).
[16] T. M. G. Mohiuddin, A. Lombardo, R. R. Nair, A. Bonetti, G. Savini, R. Jalil, N. Bonini, D. M. Basko, C. Galiotis, N. Marzari, K. S. Novoselov, A. K. Geim, and A. C. Ferrari, Phys. Rev. B **79**, 205433 (2009).

[17] M. Huang, H. Yan, C. Chen, D. Song, T. F. Heinz, and J. Hone, Proc. Natl. Acad. Sci. USA **106**, 7304 (2009).
[18] S. Berciaud, X. Li, H. Htoon, L. E. Brus, S. K. Doorn, and T. F. Heinz, Nano Lett. **13**, 3517 (2013).
[19] Z. Luo, C. Cong, J. Zhang, Q. Xiong, and T. Yu, Appl. Phys. Lett. **100**, 243107 (2012).
[20] S. Berciaud, S. Ryu, L. E. Brus, and T. F. Heinz, Nano Lett. **9**, 346 (2009).
[21] J. Maultzsch, S. Reich, and C. Thomsen, Phys. Rev. B **70**, 155403 (2004).
[22] D. Yoon, Y.-W. Son, and H. Cheong, Phys. Rev. Lett. **106**, 155502 (2011).
[23] P. Venezuela, M. Lazzeri, and F. Mauri, Phys. Rev. B **84**, 035433 (2011).
[24] D. A. Siegel, C.-H. Park, C. Hwang, J. Deslippe, A. V. Fedorov, S. G. Louie, and A. Lanzara, Proc. Natl. Acad. Sci. USA **108**, 11365 (2011).
[25] M. Lazzeri, C. Attaccalite, L. Wirtz, and F. Mauri, Phys. Rev. B **78**, 081406 (2008).
[26] W. Kohn, Phys. Rev. Lett. **2**, 393 (1959).
[27] R. Narula and S. Reich, Phys. Rev. B **87**, 115424 (2013).
[28] A. Gruneis, C. Attaccalite, L. Wirtz, H. Shiozawa, R. Saito, T. Pichler, and A. Rubio, Phys. Rev. B **78**, 205425 (2008).
[29] J. Maultzsch, S. Reich, C. Thomsen, H. Requardt, and P. Ordejón, Phys. Rev. Lett. **92**, 075501 (2004).
[30] A two-dimensional interpolation of the ingredient matrix elements and energy bands was performed first in k space and subsequently in $\boldsymbol{q}$ space using the bicubic method of Akima [41] as implemented in the freely available FORTRAN code. The $\mathcal{T}_{fi}[\boldsymbol{q}]$ corresponding to each $\boldsymbol{q}$ were calculated independently using a self-written parallel code written in FORTRAN.
[31] The averaged mode frequencies were calculated as $\omega_{2D} = \frac{|\mathcal{T}_{fi}[\boldsymbol{q}]|^2 \omega_{2D}[\boldsymbol{q}]}{|\mathcal{T}_{fi}[\boldsymbol{q}]|^2}$.
[32] The FWHM was determined by fitting the calculated spectra with two Lorentzians and then adding their individual FWHMs normalized by their area (spectral weight) of their respective peaks.
[33] Of course, the final spectra spectra shall be identical to the shown spectra apart from an intensity normalization factor of 2.
[34] The line shape for the idealized "flat *TO*" case is completely determined by the spectral response of the Raman spectrometer which is taken to be Lorentzian with a FWHM $= 1\text{cm}^{-1}$ in this work .
[35] D. L. Miller, K. D. Kubista, G. M. Rutter, M. Ruan, W. A. de Heer, P. N. First, and J. A. Stroscio, Science **324**, 924 (2009).
[36] The slope $\alpha_{\boldsymbol{K}}$ was calculated by taking the average of the slopes along the $\boldsymbol{\Gamma}$-$\boldsymbol{K}$ and $\boldsymbol{K}$-$\boldsymbol{M}$ high-symmetry directions.
[37] S. Piscanec, M. Lazzeri, F. Mauri, A. C. Ferrari, and J. Robertson, Phys. Rev. Lett. **93**, 185503 (2004).
[38] Z. Yao, C. L. Kane, and C. Dekker, Phys. Rev. Lett. **84**, 2941 (2000).
[39] A. Gruneis, J. Serrano, A. Bosak, M. Lazzeri, S. L. Molodtsov, L. Wirtz, C. Attaccalite, M. Krisch, A. Rubio, F. Mauri, and T. Pichler, Phys. Rev. B **80**, 085423 (2009).
[40] C. D. Spataru, M. A. Cazalilla, A. Rubio, L. X. Benedict, P. M. Echenique, and S. G. Louie, Phys. Rev. Lett. **87**, 246405 (2001).
[41] H. Akima, Commun. ACM **17**, 18 (1974).